Available online at www.sciencedirect.com
ScienceDirect
Ceramics International 37 (2011) 771–777
CERAMICS INTERNATIONAL
www.elsevier.com/locate/ceramint

Combined zirconia toughened alumina (ZTA) stacks obtained by electron beam physical vapour deposition

S.M. Naga [a,*], S.H. Kenawy [a], M. Awaad [a], E. Roos [b], A. Lyutovich [b], H. Ruoff [b], R. Krisch [b]

[a] Ceramic Department, National Research Centre, 12622 Dokki, Cairo, Egypt
[b] Material Testing Institute, University of Stuttgart, Germany

Received 24 May 2010; received in revised form 27 July 2010; accepted 7 October 2010
Available online 18 November 2010

Abstract

Ion assisted electron beam physical vapour deposition (EB-PVD) technique was used for three zirconia toughened alumina (ZTA) batches containing 15, 25, 35, mole% ZrO_2 and c-zirconia ceramic multilayer deposition on 617-Ni based alloy substrate. The ceramic batches were prepared via sol–gel technique. The thickness of the coated layers was found to be 0.66 μm for ZTA layers and 0.65 μm for c-zirconia layer. Evaluation of the microstructure of the samples coated with c-zirconia on the top of different ZTA coats reveals three different regions. First region indicates c-ZrO_2 coat, second region exhibits ZTA layers, while third is the metallic substrate. The top coat microstructure can be divided into two zones. The inner zone (ZTA zone), which is the early part of multiple nucleation and subsequent growth of the columnar microstructure. The outer zone (c-ZrO_2) which is crystallographically perfect columnar YSZ coatings produced by EB-PVD.

Keywords: Electron beam physical vapour deposition (EB-PVD); Zirconia toughened alumina (ZTA); Multilayered coating; Microstructure

1. Introduction

Thermal barrier coatings (TBCs) systems typically consist of a metallic oxidation protection layer and an isolative ceramic topcoat. The selection of TBC materials is restricted by some basic requirements: (1) high melting point, (2) no phase transformation between room temperature and operation temperature, (3) low thermal conductivity, (4) chemical inertness, (5) thermal expansion match with the metallic substrate, (6) good adherence to the metallic substrate and (7) low sintering rate of the porous microstructure [1,2].

Currently, two processes are widely used to produce the topcoat of these systems, electron beam physical vapour deposition (EB-PVD) and atmospheric plasma spraying (APS) [3]. However, for more than a decade, the preference is in applying TBC by EB-PVD as it offers superior thermo-mechanical properties and lifetime performance over plasma spray process.

For the next generation of TBCs, a further increase in the turbine inlet gas temperature is expected to reach a level where the commonly used partially stabilized zirconia (PSZ) material suffers from severe problems such as sintering and phase stability. TBCs produced by EB-PVD show decomposition of the metastable t-phase into monoclinic and cubic phase after 200 h at 1200 °C [4], which is common temperature level for the outer layer of current TBCs. During cooling the t′-zirconia phase with further transform into the m-phase, giving rise to the formation of microcracks in the coating [5]. Furthermore, due to the sintering of the coating at elevated temperatures, the porosity reduction is combined with the increase of Young's modulus and tensile stress, which leads to a reduced life under thermal cycling load [6].

The durability and reliability of TBCs critically depends on phenomena associated with the evolution of alumina at the interface between the metallic substrate and the insulating ceramic surface [7]. This so-called ''thermally grown oxide'' (TGO) provides the basic protection against high-temperature oxidation, but it is also the main source of strain incompatibility that can drive coating spallation on thermal cycling, as well as of defects that can initiate the failure process. The formation of mixed Al_2O_3–ZrO_2–TGO layer in TBC systems has been an intriguing subject since first identified by Stiger et al. [8]. Unal et al. [9] studied the microstructure of Y_2O_3 stabilized ZrO_2

* Corresponding author. Tel.: +20 2 333 37 143; fax: +20 2 333 70 931.
E-mail address: salmanaga@yahoo.com (S.M. Naga).

0272-8842/$36.00
doi:10.1016/j.ceramint.2010.10.030

TBCs formed by EB-PVD on a Ni-base superalloy. They showed that the thermodynamically stable α-Al_2O_3 is the dominant phase of the oxide scale formed at the TBC/bond coat interface. The morphology and distribution of α-Al_2O_3 and fine-grained ZrO_2–Y_2O_3 at the interface can be controlled through modification in the deposition procedure and the bond coat.

To overcome the disadvantages of yttria stabilized zirconia (YSZ), the multilayer and graded structures have been produced [10]. The graded coatings start with a 1 μm layer of pure Al_2O_3 that functions as an oxygen diffusion barrier and quickly transition to 7% yttria-stabilized zirconia as first described by Schultz et al. [11]. A continuously graded layer between bond coat and zirconia would lower the stresses at the interface substantially. Such systems have been described for EB-PVD [12], but it is obvious that they are limited in their potential application. Graded bond coat-zirconia layers showed improved performance under pure thermal cycling conditions but they suffer from rapid oxidation of bond coat particles in the zirconia due to their high surface area under oxidizing conditions. A study carried out by Kelly et al. [13] showed that multilayer 7YSZ and Al_2O_3 coatings with fixed layer spacing showed a 73% infrared reflectance maxima at 1.85 μm wavelength. They suggested that coating reflectance can be tailored to achieve increased reflectance over a desired wavelength range by controlling the thickness of the individual layers. Multimaterial coatings with different refractive indices cause photon scattering obeying Snell's law. Each layer in the structure causes destructive interface to wavelengths that are odd integer multiples of the half-layer thickness and constructive interference to wavelengths that are even integer multiples of the half-layer thickness.

Our coating design aims to combine the good thermal insulation of stabilized zirconia with the low diffusivity of alumina. In the present approach, zirconia toughened alumina with different zirconia concentrations was evaporated and deposited as successive layers on a 617-Ni based alloy substrate. To avoid the possible delamination between the layers, ceramic coatings have been generated by increasing the exchange of alumina by zirconia in the direction towards the coating surface.

2. Materials and methods

2.1. Preparation of the starting materials

1. The materials used for this investigation were zirconium *n*-(IV) butoxide (Strem Chemicals, Newburyport, MA, USA), aluminium tri-isopropoxide (Merck, Germany) and Y_2O_3 powder (99.99%, Strem chemicals, Newburyport, MA, USA).
2. Fully and partially stabilized zirconia powders were prepared via sol gel technique by the hydrolysis of zirconium *n*-butoxide with the addition of 8 and 5 mol.% Y_2O_3 respectively. Alumina was prepared by sol–gel technique by the hydrolysis of aluminium tri-isopropoxide then peptization with nitric acid. The dried gels were calcined at 600 °C to remove all the nitrate and organic species. Fully and partially stabilized zirconia powders were then fired at 1650 and 1500 °C respectively while alumina was fired at 800 °C. The fired powders were ground in an automatic agate mortar (Fritsch, Germany) to less than 10 μm (BET surface analysis method)
3. Zirconia toughened alumina batches were formed by combining alumina and partially stabilized zirconia. Three ZTA batches containing 15, 25, 35, mole% ZrO_2 and c-zirconia were prepared using the synthesized gel.

2.2. Preparation of EB-PVD targets

Targets were formed by casting technique. About 25 g of powder was mixed with 4.5–5 ml deionised water to give viscous paste and then poured into a conical mould with analogous shape of EB-PVD crucible. The targets were dried at 110 °C and sintered at 1650 °C to give as much high-density compacts as possible for EB-PVD deposition.

2.3. Ion assisted electron beam physical vapour deposition (IA EBPVD)

ZTA-15, ZTA 25, ZTA-35, and cubic zirconia-coatings were deposited by ion assisted electron beam evaporation on 617-nickel based alloy substrates Fig. 1. The vacuum in the chamber was 5×10^{-6} mbar. The coating process was carried out at 500 °C and 600 °C. The emission current of the e-gun was in the range from 30 mA to 50 mA depending on the kind of material to be evaporated. The bias potential was 0 V and 300 V. The distance between the melt to the substrate was 150 mm. More details of the deposition experiments are described in Ref. [14]. The thickness of the deposited films was measured by weighting the substrate and the samples after coating and with direct SEM examinations of cross-sections. The morphology of the films was studied using optical microscopy (OM), and scanning electron microscopy (SEM). The distribution of the elements in the system coatings/interface/substrate was measured using line-scan electron probe on the cross-sections of the samples.

2.4. Multilayered coating preparation

Multilayered coatings were produced as follows: the substrate was first coated with 15 mol% ZTA layer. On this layer 25 mol% ZTA followed by 35 mol% ZTA coats were deposited. A top coat was produced using 100% c-ZrO_2 coat. Fig. 2 shows a schematic representation of multilayered coatings obtained by EB-PVD technique.

2.5. Characterization

XRD analyses of powdered samples (Philips 1730 diffractometer with a Ni-filtered and monochromated Cu Kα radiation) were applied to identify crystalline phases with goniometric range 20–80° and scan speed of 1°/min. Care was taken to maintain the current at 40 kV and 40 mA during the experiment.

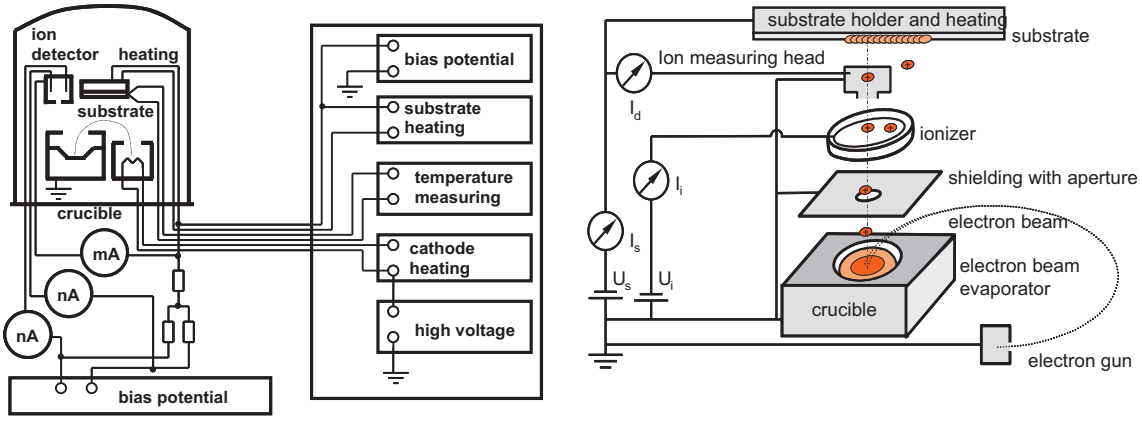

Fig. 1. Schematic representation of IA EB PVD.

TEM (Jeol 1230, Japan) was conducted on the prepared powders to examine their grain size. The morphological and microstructural characteristics were evaluated by optical microscopy as well as, the scanning electron microscope (Jeol). The Thermal analysis of the powdered samples was carried out using thermal analyser (SDT Q 600 V20.5 Build 15 USA) with a heating rate of 10 °C/min using alumina as a reference material.

3. Results and discussion

3.1. Starting materials characterization

The TEM micrograph Fig. 3a and b of the alumina gel calcined at 800 °C for 1 h showed that its grain size is in the range of 8–15 nm, while that of ZTA is in the range of 15–30 nm with a narrow size distribution. The ED pattern of the alumina powder indicates its crystallization as a monocrystals.

The TGA and DTA curves of the Al_2O_3 gel are shown in Fig. 4. There is an initial weight loss of ≈10.5% up to 125 °C due to absorbed moisture, followed by a major weight loss ≈31% between 125 °C and 500 °C that is attributed to the decomposition of the boehmite and the nitrates. Decomposition of boehmite is complete at 500 °C.

The DTA figure of the alumina gel calcined at 800 °C, Fig. 5, shows an endothermic peak at 68 °C corresponding to the removal of the mechanical water and alcohol. Two endothermic peaks at about 290 °C and 332 °C are also observed. These peaks are due to the removal of organic materials and hydroxyl groups that associated with zirconia. The broad peak at 550–650 °C is corresponding to the removal of nitrate species. TGA curve shows a total weight loss of about 49% due to the removal of abovementioned species. The crystallization of zirconia in the tetragonal form is indicated by an exothermic peak at about 1030 °C.

XRD analysis Fig. 6 shows that complete crystallization into α-alumina form (corundum) took place at 800 °C. In case of zirconia toughened alumina material, the XRD shows α-alumina phase and t- and c-ZrO_2 mixture with slight shift towards the t-phase. No other crystalline phases were detected under the conditions of the experiment. On the other hand, the XRD curve of the prepared zirconia calcined at 800 °C shows that it is completely composed of c-ZrO_2 phase.

The successive layer coatings are shown in Fig. 7. Fig. 8A shows the surface of single layer ZTA coat containing 15 mol% ZrO_2. It shows a homogeneous coat surface with approximately no open porosity. The white spots may be attributed to the Al_2O_3 grains. Such coating; with no open pores; will prevent the metallic substrate from oxidation and attack of corrosive gases.

Fig. 8B and C presents the micrograph of first and second ZTA splats on the metallic substrate. It shows a coat defect which may be caused by problems associated with spraying process (such as residual stress, and inter splats defects) or even test problems, as sample alignment or traction speed. According to Sobolev et al. [15], interlocking (and then adhesion) increases with an increase in the density and velocity of the impinging ceramic droplet. They stated that at high particle velocities the particles come so close to the substrate accordingly, interatomic bonding can occur. Rebonding of partially melted particles and stress relaxation from local plastic deformation can influence the adhesion.

SEM observations of the ZTA three layers coat are summarized in Fig. 8D. The most significant note is the presence of a continuous layer of dense ZTA. The same

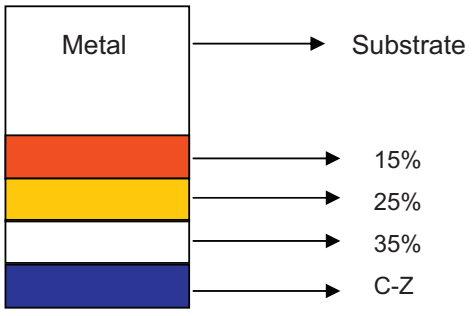

Fig. 2. Multilayered coatings on 617-Ni based alloy substrate.

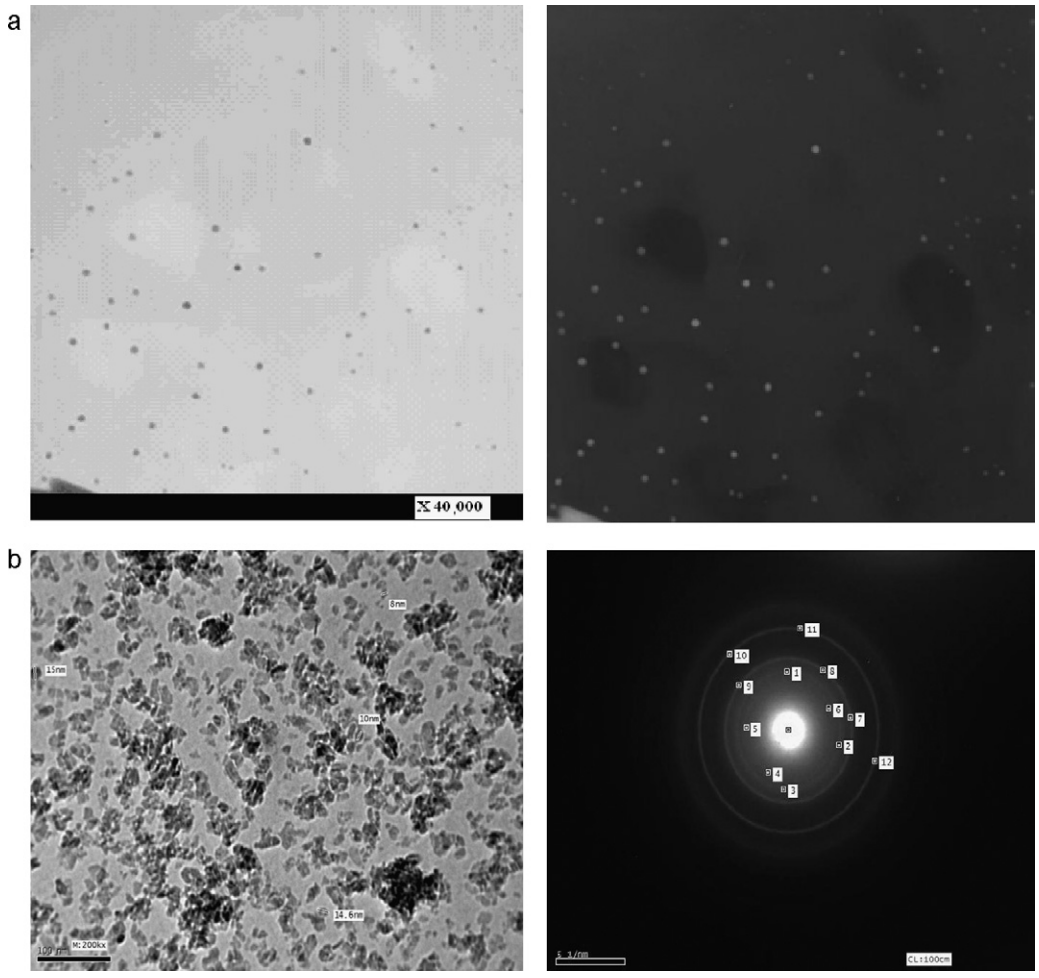

Fig. 3. (A) TEM of ZTA (40,000×) 15 up to 30 nm. (B) TEM micrographs and the corresponding ED pattern of the alumina gel calcined at 800 °C.

micrograph shows a thin layer of plastic deformation zone with a river-like microstructure along the coat/substrate interface. The fracture cross section of the ceramic coat shows a typical lamellar structure.

Evaluation of the microstructure of the samples coated with c-zirconia on the top of different ZTA coats reveals three different regions, Fig. 8E. White region indicates c-ZrO_2 coat, dark grey region exhibits ZTA layers, while light grey is the metallic substrate. The top coat microstructure can be divided into two zones. The inner zone (ZTA zone), which is the early part of multiple nucleation and subsequent growth of the columnar microstructure. The ceramic growth is strongly

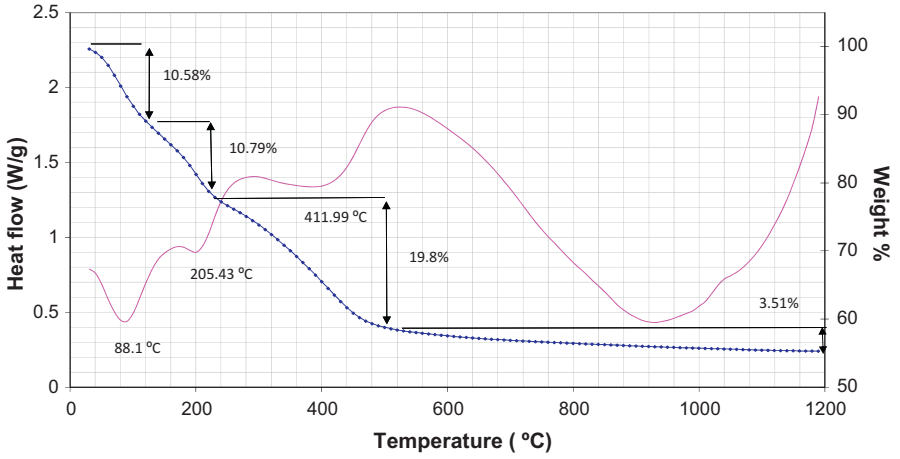

Fig. 4. The TGA and DTA curves of the Al_2O_3 gel.

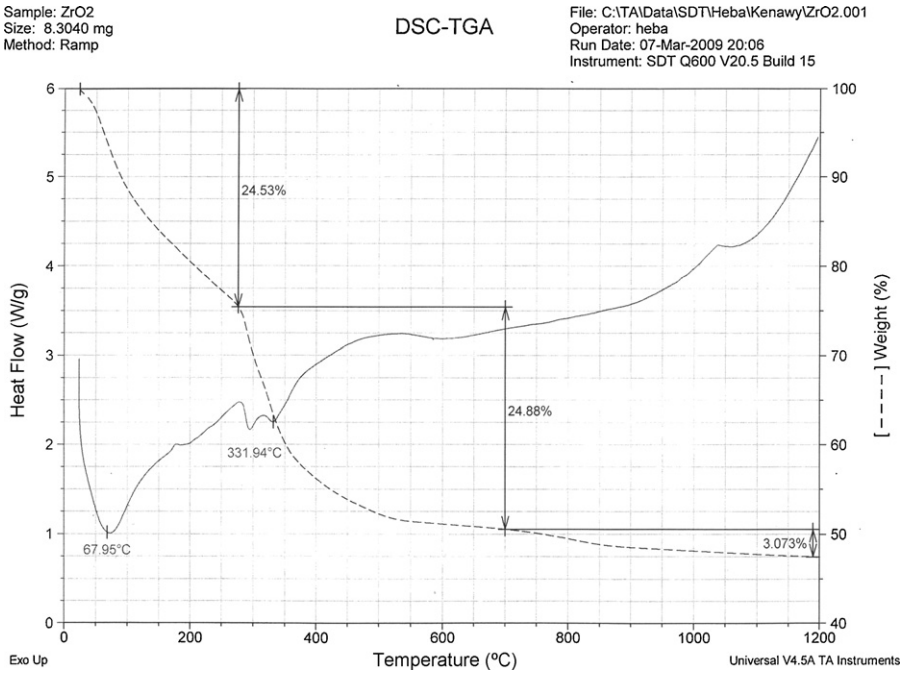

Fig. 5. TGA and DTA curves of the zirconia gel.

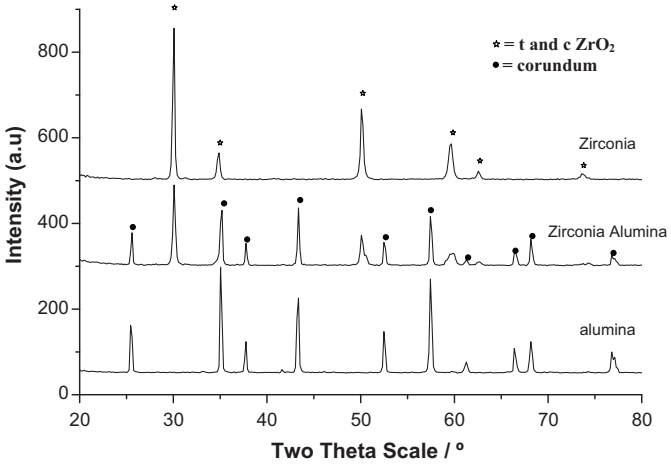

Fig. 6. XRD patterns of the synthesized powders.

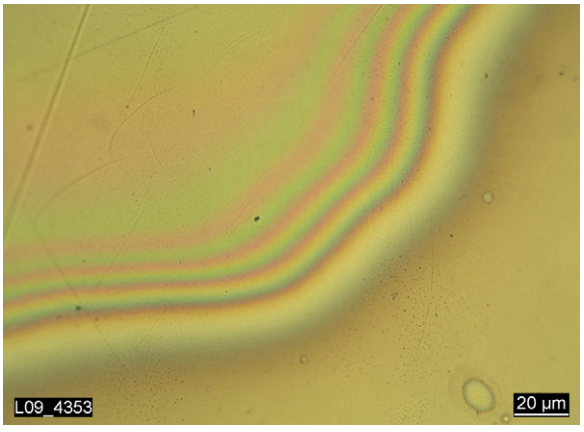

Fig. 7. Optical micrograph of the coated layers.

columnar and associated with a noticeable inter-columnar porosity. The porosity itself is strongly anisotropic and generally oriented perpendicular to the coating surface. The outer zone (c-ZrO_2) which is crystallographically perfect columnar YSZ coatings produced by EB-PVD. SEM micrograph of the sample surface, reveals very fine zirconia grains, bubble-like zirconia aggregates and micro pores Fig. 8F.

3.2. Pore size and pore diameter

Table 1 shows the different coat layers total porosity, average pore diameter and pore area. It could be shown that the coat layer containing 15 mol% ZrO_2 is dense with 1.35% porosity. The low intensity of porosity is because of the small size of Al_2O_3 powder which compose 85 wt.% of the sample. High alumina particle velocity and hence, high kinetic energy, leads to extreme plastic deformation of small particles during their collision with the substrate which in turn, reduce the gaps between the deformed particles. Furthermore, because of high velocity of powders, there is not enough time for trapping any gas inside the coating. The amount of porosity increases with increasing the zirconia content from 1.35% in 15 mol% ZrO_2 to 4.71% in 100% c-ZrO_2. It is due to the fact that during coating process particles of zirconia are not thoroughly melted, which result less plastic deformation upon collision with the substrate surface [16]. The diameter of all the coatings surface connected pores are less than 10 μm. These fine pores with a size smaller than 0.012 μm are attributed to the small voids originated from gas entrapment, the microcracks and the macropores formed in interpolates. We suggested that decreased porosity might lead to better optimization of thermomechanical behavior, especially during thermal cycling.

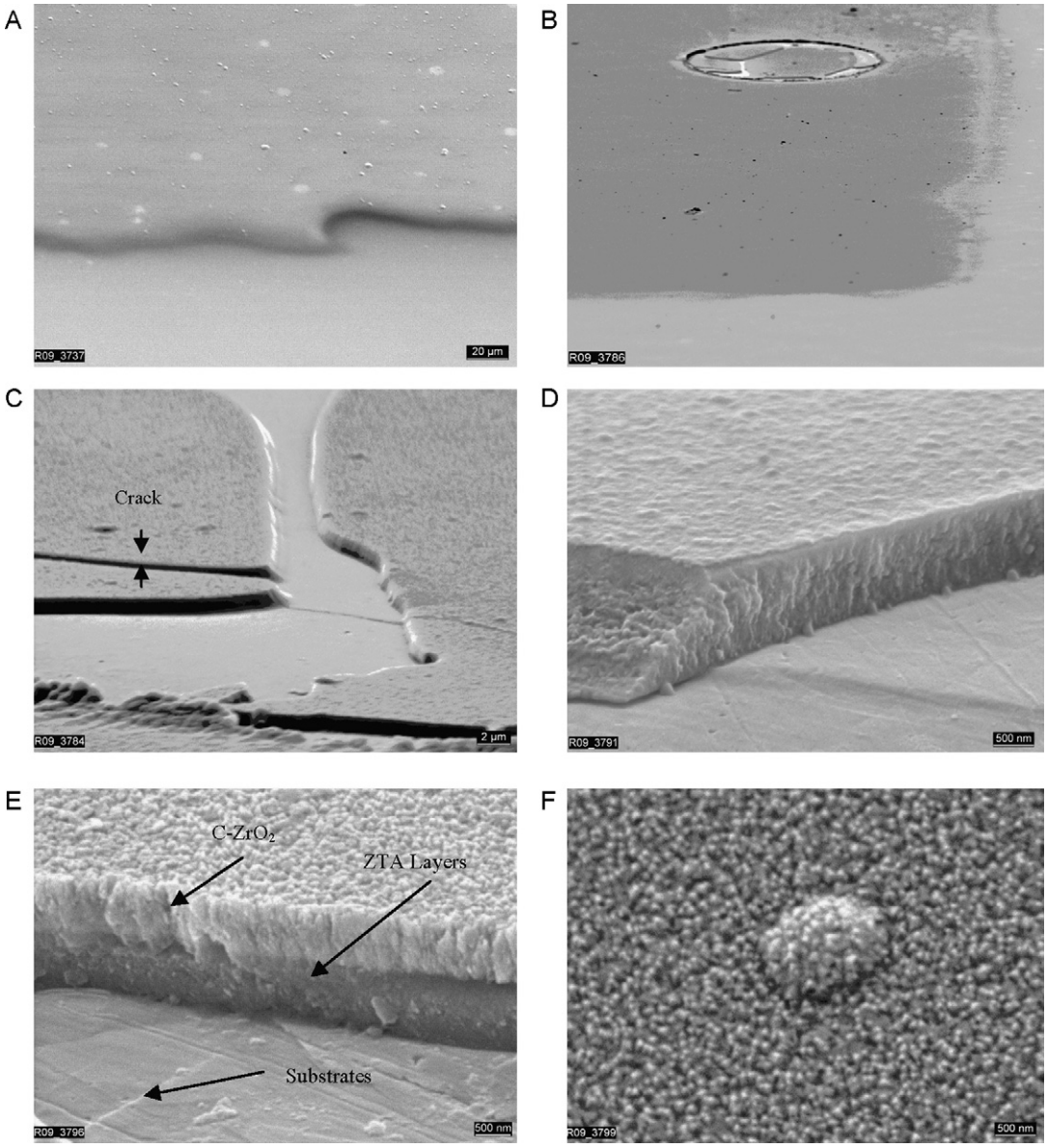

Fig. 8. (A) First ZTA ceramic layer coat on 617-Ni based alloy with 15 mol % ZrO_2 content. (B and C) ZTA second layer coat showing plastic deformation and crack propagation. (D) Three layers of ZTA coat. (E and F) ZTA with 15, 25, 35 mol% ZrO_2 and c-zirconia top coat.

Table 1
Total porosity and pore diameter of the ceramic coat.

Sample ID	Total intrusion Volume, ml/g	Total pore area, m^2/g	Average pore Diameter, μm	Total porosity, %
15 mol% ZrO_2	0.0012	0.498	0.011	1.35
15 + 25 mol% ZrO_2	0.0043	1.429	0.011	3.90
15 + 25 + 35 mol% ZrO_2	0.0046	1.700	0.012	4.13
15 + 25 + 35 mol% ZrO_2 + c-ZrO_2	0.0055	2.654	0.008	4.71

4. Conclusions

1. The porosity of the ZTA/c-ZrO_2 graded composite coating was found to decrease from surface towards the coating near the substrate.
2. Multilayer coat microstructure reveals three different regions: c-ZrO_2, ZTA layer and metallic substrate.
3. The top coat microstructure can be divided into two zones, the inner zone (ZTA zone) and outer zone (c-ZrO_2). The ceramic growth is strongly columnar and associated with inter-columnar anisotropic porosity perpendicular to the coating surface.
4. The outer zone is consisted of crystallographically perfect columnar YSZ coating. SEM micrograph of the sample

surface, reveals very fine zirconia grains, bubble-like zirconia aggregates and micro pores

5. The thickness of the coated layers was found to be 0.66 μm for ZTA layers and 0.65 μm for c-zirconia layer.

References

[1] F. Cernuschi, P. Bianchi, M. Leoni, P. Scardi, Thermal diffusivity/microstructure relationship in Y-PSZ thermal barrier coatings, J. Therm. Spray Technol. 8 (1) (1999) 102–109.

[2] D. Marcin, T. Jeanine, D.K. Gupta, Protection coatings in the gas turbine engine, Surf. Coat. Technol. 68/69 (1994) 1–9.

[3] D. Stöver, C. Funke, Directions of the development of thermal barrier coatings in energy applications, Mater. Proc. Technol. 92 (93) (1999) 195–202.

[4] U. Schulz, Phase transformation in EB-PVD yttria partially stabilized zirconia thermal barrier coatings during annealing, J. Am. Ceram. Soc. 83 (4) (2000) 904–910.

[5] R. Vaβen, F. Tietz, G. Kerkhoff, D. Stöver, in: J. Lecomte-Beckers, F. Schuber, P.J. Ennis (Eds.), Proceedings of the 6th Liège Conference on Materials for Advanced Power Engineering, vol. 3, Forschungszentrum Jülich GmbH, Jülich, Germany, 1998, p. 1627.

[6] H. Dai, X. Zhong, J. Li, Y. Zhang, J. Meng, X. Cao, Thermal stability of double-ceramic-layer thermal barrier coatings with various coating thickness, Mater. Sci. Eng. A 433 (2006) 1–7.

[7] A.G. Evans, D.R. Mumm, J.W. Hutchinson, G.H. Meier, F.S. Pettit, Mechanisms controlling the durability of thermal barrier coatings, Prog. Mater. Sci. 46 (5) (2001) 505–553.

[8] M.J. Stiger, N.M. Yanar, F.S. Pettit, G.H. Meier, Mechanisms for the failure of electron beam physical vapour deposited thermal barrier coatings induced by high temperature oxidation, in: J.M. Hampikian, N.B. Dahotre (Eds.), Elevated Temperature Coatings: Science and Technology III, The Minerals, Metals and Materials Society, Warrendale, PA, 1999, pp. 51–65.

[9] O. Unal, T.E. Mitchell, A.H. Heuer, Microstructure of Y_2O_3-stabilized ZrO_2 electron beam-physical vapor deposition coatings on Ni-base superalloys, J. Am. Ceram. Soc. 77 (4) (1994) 984–992.

[10] X.Q. Cao, R. Vaβen, F. Tietz, D. Stöver, New double-ceramic layer thermal barrier coatings based on zirconia-rare earth composite oxides, J. Eur. Ceram. Soc. 26 (3) (2006) 247–251.

[11] U. Schultz, T. Krell, U. Leushake, M. Peters, Graded design of EB-PVD thermal barrier coating systems, in: Proceedings of the 85th Meeting of the AGARD Structures and Materials Panel, Aalborg, Denmark, October, 1997, pp. 16-1–16-10.

[12] F. Jamarani, M. Korotkin, R.V. Lange, M.F. Ouelette, K.L. Yan, R.W. Bertram, V.R. Parameswaram, Compositionally graded thermal barrier coatings for high temperature aero gas turbine components, Surf. Coat. Technol. 54/55 (1) (1992) 58–63.

[13] M.J. Kelly, D.E. Wolfe, J. Singh, J. Eldridge, D.-M. Zhu, R. Miller, Thermal barrier coatings design with increased reflectivity and lower thermal conductivity for high-temperature turbine applications, Int. J. Appl. Ceram. Technol. 3 (2) (2006) 81–93.

[14] E. Roos, K. Maile, A. Lyutovich, A. Gusko, A. Udoh, (Cr–Al) bi-layer coating obtained by ion assisted EBOVD on C/C–SiC composites and Ni-based alloys, Surf. Coat. Technol. 151–152 (2002) 429–433.

[15] V.V. Sobolev, J.M. Guilemany, J. Nutting, J.R. Miquel, Development of substrate-coating adhesion in thermal spraying, Int. Mater. Rev. 42 (3) (1997) 117–136.

[16] A.M. Khoddami, A. Sabour, S.M.M. Hadavi, Microstructure formation in thermally-sprayed duplex and functionally graded NiCrAlY/yttria-stabilized zirconia coatings, Surf. Coat. Technol. 201 (12) (2007) 6019–6024.